UCRL- 1440

UNCLASSIFIED

UNIVERSITY OF CALIFORNIA — BERKELEY

TWO-WEEK LOAN COPY

This is a Library Circulating Copy which may be borrowed for two weeks. For a personal retention copy, call Tech. Info. Division, Ext. 5545

RADIATION LABORATORY

DISCLAIMER

This document was prepared as an account of work sponsored by the United States Government. While this document is believed to contain correct information, neither the United States Government nor any agency thereof, nor the Regents of the University of California, nor any of their employees, makes any warranty, express or implied, or assumes any legal responsibility for the accuracy, completeness, or usefulness of any information, apparatus, product, or process disclosed, or represents that its use would not infringe privately owned rights. Reference herein to any specific commercial product, process, or service by its trade name, trademark, manufacturer, or otherwise, does not necessarily constitute or imply its endorsement, recommendation, or favoring by the United States Government or any agency thereof, or the Regents of the University of California. The views and opinions of authors expressed herein do not necessarily state or reflect those of the United States Government or any agency thereof or the Regents of the University of California.

UNCLASSIFIED

UCRL-1440
Unclassified-Physics Distribution

UNIVERSITY OF CALIFORNIA

Radiation Laboratory

Contract No. W-7405-eng-48

EXPERIMENTS ON ELASTIC SCATTERING OF 190-MEV DEUTERONS BY PROTONS

Martin O. Stern

(Thesis)

August, 1951

Berkeley, California

INDEX

SECTION		PAGE
I	Summary	3
II	Introduction	4
III	Experimental Arrangement	8
IV	Kinematics and Geometry	11
V	Experimental Procedure	17
VI	Sample Calculation	25
VII	Presentation of Data and Discussion of Errors	29
VIII	Conclusions	35
IX	Acknowledgments	40
X	Appendix: The Carbon Subtraction Ratio	41
XI	References	44
XII	Figures	46

EXPERIMENTS ON ELASTIC SCATTERING OF 190-MEV DEUTERONS BY PROTONS

Martin O. Stern

Radiation Laboratory and Department of Physics
University of California, Berkeley, California

August, 1951

I SUMMARY

The elastic differential scattering cross section of 190-Mev deuterons by protons has been measured from 15° to 170° in the center of mass system. The cross sections were obtained by subtracting the carbon counts from those received with a polyethylene target. A scintillation coincidence counting technique was used over most of the range of angles measured. Results are shown in Table II and Figs. 12 and 13, and compared with those predicted by Chew.[1]

II INTRODUCTION

Scattering experiments constitute one of the most powerful tools for investigating nuclear forces. We are interested in the general nature of these forces, i.e., their origin, their connection with mesons, etc., and in the interaction between various kinds of nucleons, i.e., in the relative strenghts of n-p, p-p, and n-n forces, and the phases of the scattered waves resulting from them. Presumably, a complete knowledge of these would enable one to predict the outcome of all scattering experiments and to foretell the binding energies, radioactivities and energy levels of all nuclei. Evidently relativistic effects will greatly complicate the theory for very high energy scattering. We shall therefore restrict ourselves for the moment to energies where relativistic effects are expected to play a minor role. It is symptomatic of our state of ignorance of nuclear forces that even within this restricted frame it has so far been extremely difficult to reconcile the results from any two, let alone all three, of the sources of information mentioned below.

Our first source comes from an inspection of the binding energies and decay characteristics of light nuclei.[2] Here we find, in connection with our problem, first, that nuclear forces must lead to saturation; second, that n-n and p-p forces in light nuclei are about the same, and neither very much weaker, nor much stronger, than n-p forces.

The second source of information comes from a consideration of low-energy nucleon-nucleon scattering and from our knowledge of the bound state of the deuteron. If the energy is low enough, only the partial S wave contributes appreciably to the scattering, and it is well known that in this region scattering experiments give only two parameters[3] of the interaction potential, say its effective range[4] and scattering length at zero energy.[5]

From the theory of the deuteron,[2] and from experiments on neutron-proton,[6] proton-proton[7] and neutron-parahydrogen[8,9,10] scattering at very low energies the four parameters of singlet and triplet potentials can be found. In particular, both potentials are attractive, but have different depths, the singlet well being shallower than the triplet well. This shows that spin-dependent forces contribute to some extent to the nuclear interaction at low energies.

At somewhat higher energies, where partial S-waves are still predominant, the shape of the tail of the well begins to be felt, so that the choice of radial potentials has to be restricted slightly if the charge independence of nuclear forces is to be preserved. It has been shown[11] that under the above assumptions a Yukawa type potential yields a good fit with all the experimental low energy data. The potentials taken are $V^s(r) = \frac{A_s}{\alpha_s r} e^{-\alpha_s r}$, $V^t(r) = \frac{A_t}{\alpha_t r} e^{-\alpha_t r}$, where $V^s(r)$, $V^t(r)$ are the singlet and triplet potentials, respectively, A_s, A_t the well depths, α_s, α_t the ranges. For the best fit the values adopted[11,12] for the parameters are $\alpha_s = \alpha_t = 0.42 \frac{e^2}{mc^2} = 1.18 \cdot 10^{-13} cm^{-1}$, $A_s = -46.5$ Mev, $A_t = -67.8$ Mev.

Our third source of information comes from a study of high energy nucleon-nucleon scattering. It is found that the experimental data in this region[13-17] cannot be fitted with the ordinary or Wigner type potentials $V^s(r)$ and $V^t(r)$. In particular, the cross section calculated from them is higher than the observed one in the n-p case, lower than the observed one in the p-p case, and has the wrong shape in both cases. Several remedies suggest themselves. The simplest is that some of the higher angular momenta do not contribute to the scattering. Indeed it has been shown by Christian and Hart,[18] working at Berkeley with Professor Serber, that if the n-p potential is half ordinary, half Majorana exchange, i.e. of the form $\frac{A}{\alpha r} e^{-\alpha r} \frac{1 + P}{2}$, where P is the

space exchange operator, agreement with the experimental cross section can be reached. The effect of such a "Serber potential" is to eliminate the scattering in states of odd angular momentum. Since such a potential is to be used in both singlet and triplet states, charge independence demands that in the proton-proton interaction only even states scatter, or, by the Pauli principle, only singlet states. This further lowers the calculated p-p cross section. To raise it and give it a suitable shape, a tensor interaction[19] is introduced. This will affect the calculated p-p cross section considerably without doing violence to that for n-p scattering, but even now the theoretical fit to the former is only mediocre. Clearly the foregoing alterations do not materially affect the low-energy cross sections. We have not touched the S states except for the tensor forces in n-p whose contribution can be made negligible for long wavelengths.

We are now confronted with a serious difficulty. Although we have brought low- and high-energy scattering data into moderately satisfactory agreement, the Serber potential adopted does not lead to saturation, since odd angular momenta do not result in repulsion, but merely in zero interaction. To overcome this difficulty, Jastrow[20] has suggested the introduction of a repulsive core in the singlet nucleon-nucleon potential. The effect of such a potential would be that the singlet S phase shift would change sign somewhere in the high energy region. One might also adopt partially non-static forces in which the potentials are functions of the angular momenta ℓ, or of $\ell \cdot \sigma$.[21] It is only after exhausting every aspect of these possibilities that one would, very reluctantly, have to give up the basic concept of the charge independence of nuclear forces.

Evidently a solution to these problems can be sought with greater chance

of success if more experimental information is obtained. Here we may mention the following:

1) More accurate differential cross sections for n-p and p-p scattering at well-known low energies are needed.[6,7]

2) Experiments should be carried out to test the equality of n-n and p-p forces at intermediate and high energies.

3) Interference experiments of the parahydrogen type[8,9] should be attempted to correlate the signs of the phase shifts in n-p, n-n, and p-p scattering at various energies.

As to 2): here neutron targets are not available. The next best thing is to measure the n-d and p-d cross sections; n-d scattering has been carried out by Powell[17] using 90 Mev neutrons (with an unavoidably broad energy spectrum). A more monochromatic neutron beam would be highly desirable here. The theory has been treated by Chew,[22] and Gluckstern and Bethe.[23] As to 3): here we use the deuteron in lieu of parahydrogen. d-p and n-d elastic scattering at low energies have been carried out.[24-28] If the energy used is higher, the deuteron will evidently break up a good fraction of the time; but since the elastic effect can easily be separated from the inelastic, experiments in this energy region are useful in giving us a greater knowledge of the potentials involved, especially in the region where the Born approximation becomes valid.

For this reason it is of value to perform p-p, n-p, n-d and d-p experiments in the high energy region. The present experiment is part of a program which has included p-p experiments in the neighborhood of 100 Mev by Birge et al,[13] and at various high energies by Chamberlain, Segrè and Wiegand;[14] n-p experiments at 90 Mev by Hadley et al;[16] and n-d scattering at 90 Mev by Powell.[17] Inelastic d-p measurements at 190 Mev by A. L. Bloom are still in progress.

III EXPERIMENTAL ARRANGEMENT

A plan of the cyclotron is shown in Fig. 1. We used the full energy (about 192 Mev) deuteron beam. The ions were scattered, according to a method first proposed by Leith,[29] by multiple scattering in an internal target, and magnetically deflected out of the main tank. They passed through the field of a bending-focusing magnet, then through the concrete shielding by way of a collimator hole, and into the "cave", where the scattering apparatus was located. In all our runs a 4 foot brass collimator of circular cross section was used, with diameter 1/2 inch through most of its length, and 3/4 inch diameter through the last 15 inches. The cyclotron was pulsed 60 times a second, and during each pulse the particles were observed to emerge for from 30 to 60 μs. The beam provided by the operating crew was, in general, very steady over periods of hours at any intensity level at which we wished to operate.

The scattering apparatus was placed in the "cave" (see Fig. 1), on an adjustable platform which could be moved by remote control. This apparatus, designed by Dr. Clyde Wiegand, was previously used in high energy n-p and p-p experiments,[16,14] and will be described only briefly. It was provided with a remote control device for putting any of three targets in the beam. Two arms carrying the counters could be rotated about the target position as pivot. The angles of one arm with respect to a fixed line through the pivot and with respect to the other arm were calibrated in degrees.

By means of two quadrant ionization chambers located fore and aft the 0° line on the table could be brought in coincidence with the beam. These chambers had four quadrants facing the collection plate. Two adjacent quadrants were at high positive potential, the other two at high negative potential. It was possible, by means of a switching device, to make the diameter separating the two semicircles of opposite high potential either vertical or horizontal on

both chambers at once. Thus a null current reading indicated perfect horizontal, or perfect vertical, centering on the beam, respectively.

An argon filled ionization chamber whose collection electrode lead to a current integrator circuit[30] was used to monitor the beam and was placed, far aft of the target, on the 0° line in the beam. The counters consisted of trans-stilbene crystals (grown by Dr. R. F. Leininger to our specifications) followed by magnetically shielded 1P21 photomultipliers and distributed amplifiers.[31] Fast amplifier and coincidence equipment enabled us to keep the accidental coincidence rate low. Of the three target positions one was left blank, the other two held polyethylene (CH_2) and graphite targets of the desired thicknesses. These were taken over from the p-p experiments,[14] where they were so chosen as to have equal stopping power for 345 Mev protons: $C \approx 1.2\ CH_2$. The result for 190 Mev deuterons was that the carbon target in general had a stopping power somewhat, but less than 10 percent, higher than had the polyethylene target.

The remaining equipment was located outside the "cave." A block diagram is shown in Fig. 2. The output from a pre-amplifier was passed through a distributed amplifier, which put out pulses of about 2×10^{-8} sec. width. These went to a discriminator pulse shaper circuit designed by Mr. Arnold L. Bloom, the purpose of which was to eliminate low level noise and stabilize the pulse form to a fairly square shape of about 0.7×10^{-7} sec. width at half height. The pulses from the two "channels" were then taken directly to scalers as well as to a coincidence circuit of approximate dead time 10^{-7} sec. This output again went to a scaler. Thus it was possible to count single events as well as coincidences. The scalers had a resolving time of around 10^{-6} μs. Most of the electronics, where not otherwise specified, were of conventional design.

Four methods of operation were used. In method I the pulses from the

distributed amplifiers went directly to a fast coincidence circuit[32] whose output fed into a scaler. Methods II, III, and IV made use of the pulse shaper discriminator. In Method II two crystals were used, and their single counts and coincidences were scaled. Method III, depicted in Fig. 2, was of value whenever one arm had to be placed close to the beam, where many stray particles were to be expected. Two crystals were placed one behind the other along this arm, and the coincidence counts from these two and those from all three, as well as the single counts could be scaled. In method IV a single crystal was used. This method was helpful in the region of scattering involving large momentum transfers. All methods agreed within statistical errors in the region in which their results overlapped.

IV KINEMATICS AND GEOMETRY

1. Kinematics.

Let M be the mass of a particle incident with kinetic energy E in the laboratory system on another particle of mass m, initially at rest. The two particles collide; that of mass M is deflected to a direction Ⓗ, that of mass m, to a direction Φ, with respect to the incident beam in the laboratory system. Let θ be the angle of deflection of either particle in the center of mass system. The event is illustrated in Figs. 3a, 3b, as seen from both systems.

We define $\rho = \frac{m}{M}$, $\epsilon = \frac{E}{Mc^2}$,

$$A = \frac{\epsilon + 1 + \rho}{\left[\rho^2 + 2\rho(\epsilon + 1) + 1\right]^{1/2}} \quad \text{and} \quad B = \left[\frac{1}{\rho^2} - 1 + A^2\right]^{1/2} =$$

$$A \frac{\epsilon + 1 + \frac{1}{\rho}}{\epsilon + 1 + \rho}. \tag{1}$$

We can then derive the following relativistic relations:

$$\tan\frac{\theta}{2} = \frac{1}{A}\cot\Phi, \tag{2}$$

$$\tan\frac{\theta}{2} = \frac{1 \pm \left[1 + \tan^2 Ⓗ \left(1 - \frac{1}{\rho^2}\right)\right]^{1/2}}{\tan Ⓗ \,(B - A)} \tag{3}$$

or

$$\tan Ⓗ = \frac{2\tan\frac{\theta}{2}}{B + A + (B - A)\tan^2\frac{\theta}{2}}; \tag{3'}$$

$$E_m = 2mc^2(A^2 - 1)\sin^2\frac{\theta}{2} \quad \text{with} \tag{4}$$

$$E_M = E - E_m \tag{5}$$

by conservation of energy.

The energy available in the center of mass is:

$$E_o = \frac{E}{A} - (m + M)c^2(1 - \frac{1}{A}), \tag{6}$$

and the momenta in the center of mass are:

$$\underset{\sim}{p_o} = mc\left[A^2 - 1\right]^{1/2}(\hat{\underset{\sim}{x}}, 0\hat{\underset{\sim}{y}}), \qquad \underset{\sim}{p_f} = mc\left[A^2 - 1\right]^{1/2}(\hat{\underset{\sim}{x}}\cos\theta, \hat{\underset{\sim}{y}}\sin\theta), \tag{7}$$

where E_M, E_m are the energies of incident and struck particle in the laboratory after the collision, and E_o, $\underset{\sim}{p_o}$, $\underset{\sim}{p_f}$ the available energy, initial momentum and final momentum in the center of mass respectively. $\hat{\underset{\sim}{x}}$ and $\hat{\underset{\sim}{y}}$ are unit vectors in the scattering plane along and perpendicular to the beam.

In our case the deuteron is to be identified with M, Θ the proton with m, Φ, and $\rho = 1/2$. Then $A = \frac{\epsilon + 3}{\left[\epsilon + \frac{9}{4}\right]^{1/2}}$, $B = \frac{\epsilon + 3}{\left[\epsilon + \frac{9}{4}\right]^{1/2}}$. In presenting our results we used Eqs. (1) to (5) throughout. For purposes of discussion it is, however, sufficient to consider these relations in their non-relativistic limits, inasmuch as all corrections are slight. As $\epsilon \rightarrow 0$, we have $A = 1$ and $B = \frac{1}{\rho}$, and Eqs. (2) to (4) become:

$$\tan\frac{\theta}{2} = \cot\Phi, \tag{8}$$

$$\tan\frac{\theta}{2} = \frac{1 \pm \left[1 - (\frac{1}{\rho^2} - 1)\tan^2\Theta\right]^{1/2}}{(\frac{1}{\rho} - 1)\tan\Theta}, \tag{9}$$

or

$$\tan\Theta = \frac{2\tan\frac{\theta}{2}}{\frac{1}{\rho} + 1 + (\frac{1}{\rho} - 1)\tan^2\frac{\theta}{2}}, \tag{10}$$

and

$$E_m = 2mc^2\frac{2\epsilon}{(\rho + 1)^2}\sin^2\frac{\theta}{2} = \frac{4E\rho}{(\rho + 1)^2}\sin^2\frac{\theta}{2}. \tag{11}$$

The following are now apparent.

1) The center of mass angle is a double-valued function of the laboratory angle of deflection of the deuteron, and so, therefore, is the laboratory

angle of deflection of the proton, i.e. for each value of Θ there are two possible values of θ or Φ. Thus when $\Theta = 0^\circ$, $\theta = 0^\circ$ or 180° and $\Phi = 90^\circ$ or 0°.

2) Tan Θ may reach a maximum. This occurs when $\tan^2 \frac{\theta}{2} = \frac{1+\rho}{1-\rho}$. Thus for $\rho > 1$ no maximum occurs. For $\rho = 1$ it occurs at $\theta = \pi$, when $\Theta = \frac{\pi}{2}$. For $\rho < 1$ we obtain that $\tan \Theta \leqslant \left[\frac{1}{\rho^2} - 1\right]^{-1/2}$. For our problem this yields $\Theta \leqslant 30^\circ$. At $\Theta = 30^\circ$, $\Phi = 30^\circ$ and $\theta = 120^\circ$.

3) The energy of the struck particle is a maximum when $\theta = \pi$. It reaches E only when $\rho = 1$. In our case the maximum energy is $\frac{8}{9}$ E or about 171 Mev. It is now clear that in Eq. (9) the positive sign must hold in the region $120^\circ \leqslant \theta \leqslant 180^\circ$ and the negative sign in the region $0^\circ \leqslant \theta \leqslant 120^\circ$. In the former region $0 \leqslant \frac{E_M}{E} \leqslant 1/3$, in the latter $1/3 \leqslant \frac{E_M}{E} \leqslant 1$.

2. Targets.

At intermediate angles, say $25^\circ \leqslant \Phi \leqslant 55^\circ$, both the deuteron and the elastically scattered proton have sufficient energy so the targets can be moderately thick. CH_2 0.290 g/cm^2 and C 0.336 g/cm^2 were usually chosen here. For larger Φ, the proton energy approaches 0. There the target, which was, in the intermediate region, oriented so as to make the crystal geometry suitable, had to face the proton counter and be as thin as possible. CH_2 0.072 g/cm^2 and C 0.080 g/cm^2 were available for this region. The protons at 70° have 19 Mev energy and a range of 0.5 g Al. 70° was the highest angle that could be reached with this method. Toward small Φ, the deuteron energy becomes quite low, approaching 21 Mev or about 1/3 g Al range as $\Phi \rightarrow \theta$. Here again the same criteria apply. All the above applies to methods I-III. In method IV thicker targets had to be used.

3. Crystals.

Here two criteria, independent of one another, had to be used. Call b, c,

the distances of proton crystal at angle Φ and deuteron crystal at angle Ⓗ, from the point at which the center of the beam hits a thin target. The first criterion determines the ratio b/c, the second, b.

a) Determination of b/c. We assume that the distance b is fixed, i.e. that the proton crystal defines the solid angle. We require that the dimensions of the crystal at Ⓗ enable it to count all elastic deuterons whose partners have entered the proton crystal.

1) The required height of the deuteron crystal is shown by the construction of Fig. 3c, in which the positions of both crystals and of the beam have been projected onto a plane perpendicular to the beam. The latter is taken to be 2.0 cm in diameter, for this area has been shown, by microphotometer analysis of films, to contain better than 99 percent of the beam at a distance of about 100 cm from the cave end of the 1/2 inch - 3/4 inch collimator. We require that the partners of protons from extreme points of the beam and just barely counted in the crystal at Φ be received, with some margin of safety, by the deuteron crystal.

2) The width of the deuteron crystal is determined by three factors: the aperture $\Delta\Phi$ of the proton crystal, the beam width as projected on the target whose plane makes a given angle δ with the deuteron arm, and the thickness of the target. Since in methods I-III only thin targets were used, the third factor is never more than a few mm, and so can be neglected.

Let a be the width of the beam at the target, equal to 2 cm with a good margin of safety. Let w be the width required of the crystal at Ⓗ, x its contribution from the beam diameter a, y that from the width W of the crystal at Φ.

We have: $$x = c\,\Delta\Theta_a + \frac{a}{\sin(\delta + \Theta)}\sin\delta$$

$$= c\,\frac{d\Theta}{d\Phi}\Delta\Phi_a + \frac{a}{\sin(\delta + \Theta)}\sin\delta$$

$$= \frac{a}{\sin(\delta + \Theta)}\left[\frac{c}{b}\sin(\Theta + \Phi + \delta)\frac{d\Theta}{d\Phi} + \sin\delta\right];$$

$$y = \frac{c}{b}W\frac{d\Theta}{d\Phi} = c\,\Delta\Theta_w;$$

$$w = \frac{c}{b}\frac{d\Theta}{d\Phi}\left[W + \frac{a}{\sin(\delta + \Theta)}\sin(\Theta + \Phi + \delta)\right] + \frac{a\sin\delta}{\sin(\delta + \Theta)}; \qquad (12)$$

where for $\frac{d\Theta}{d\Phi}$ we use the non-relativistic approximation:

$$\frac{d\Theta}{d\Phi} = \frac{4\cos 2\Phi - 2}{5 - 4\cos 2\Phi}. \qquad (13)$$

b) The distance b is determined by two factors:

1) The resolution. Except at small angles, 2° to 5° was here judged sufficient.

2) The ratio of elastic counts to accidental coincidences, which was to be kept as high as possible. This demanded a low beam current, and therefore, with the finite time available, a poorer resolution. An optimum b was determined empirically for which the accidental counts per unit beam charge were reasonably low, and the charge per second still reasonably high.

The problems involved are illustrated in the sample calculation of Sec. VI. To summarize: thin targets were used with methods I-III at small and large Φ; intermediate targets in the middle region. Thicker targets were required in method IV where the background came largely from the collimator. It was found geometrically convenient to make the proton crystal, at angle Φ, the defining

one throughout in methods I-III. The solid angle subtended by the other crystal had to be made correspondingly large. Suitable checks, described below, were made to give us confidence in the criteria here developed.

V. EXPERIMENTAL PROCEDURE

We shall now describe chronologically the experimental routine used during any particular day's run at the cyclotron. We need here only distinguish between the coincidence methods (I, II, III) and the single counting method (IV).

A. COINCIDENCE METHODS

"Setting up."

The variables of cyclotron operation (main magnetic field, rotating condenser frequency, filament current, pulsed arc voltage and timing, steering and focusing magnet field, pre-magnet collimator, etc.) were adjusted to give maximum beam at the tank end of the external collimator. The latter was then adjusted in position to provide maximum current at the cave end. Photographic film was exposed to check that the collimation axis was parallel to the beam. As soon as this process was completed, the operating crew was asked to keep constant all variables that might affect the duty cycle of the cyclotron, and to vary the beam only by varying the filament current and pulsed arc voltage.

The table was next aligned by moving the platform supporting it until the beam passed through the centers of the two quadrant ionization chambers. These were then removed and the beam integration chamber inserted.

Checks.

Several checks were carried out to make sure that the equipment was functioning properly and that we were operating with suitable geometry, etc.

1) After aligning the table with quadrant chambers, films were exposed to the beam fore and aft on the table in order to check the 0° position.

2) The crystals were set at some Φ and Θ corresponding to elastic scattering. The photomultiplier potentials were adjusted to some reasonable value. The table was then raised or lowered and the coincidence counting rate was plotted as a function of height. A typical curve is shown in Fig. 4. The

flat portion was usually of the order of 1 or 2 cm wide, and since the abscissa of its center was always within 1/4 cm of the height obtained with the quadrant ionization chamber alignment, this check was only performed periodically.

3) The angle between the two counters was varied, keeping Φ fixed. The hydrogen coincidence counting rate was then plotted as a function of Θ. The correct angle setting was taken as the center of the flat portion of the curve. A typical curve is shown in Fig. 5. This method provided a third check on our line-up, or could, conversely, be taken as a check on the kinematics and hence as an identification of the scattering process. This check was almost always performed at least once, and sometimes twice at two widely separated settings.

4) For further checks it was now necessary to vary the voltage on each photomultiplier in turn, keeping that on the other one or two photomultipliers constant at a reasonable value, and plot the hydrogen coincidence rate as a function of voltage. A typical curve is shown in Fig. 6. The hydrogen effect, obtained by subtraction of carbon from CH_2, had to be used inasmuch as the accidental coincidences from carbon, probably including charged particles of various energies, gamma rays, electrons, neutrons, etc., could not be expected to give a counting plateau.

5) Various thicknesses of aluminum absorbers were placed in front of one or the other crystal and the hydrogen effect was observed as a function of absorber thickness. A plot of such a test is shown in Fig. 7. This test was carried out only a few times inasmuch as the amount of absorber required to make the effect disappear was always in agreement with the energy calculated for the elastic process.

6) The energy of the beam was measured by measuring the ratios of the currents of two ionization chambers placed in the beam with a variable amount of aluminum absorber between them. A typical plot of current ratio versus

absorber is shown in Fig. 8. This test was carri out several times, and the beam energy was always the same within the accuracy of the experiment, i.e., 192 $\pm$ 2 Mev, while the straggling seemed to vary somewhat.

7) The distance c of the non-defining deuteron crystal at angle Ⓗ was varied, and the hydrogen effect was observed as a function of c. This test was performed several times at various angles and the result convinced us that our geometry contained a sufficient safety factor.

8) Whenever we had to go to large or small Φ where thinner targets had to be used, the target change was made at such an angle that the hydrogen effect was the same with thick and thinner target. We thus convinced ourselves that, except possibly at $\Phi = 70^{\circ}$, all of the low energy particles were able to reach their crystal and be counted.

Carbon subtraction.

At a given set of angles Φ and Ⓗ corresponding to elastic hydrogen scattering from CH_2 we counted not only the elastic hydrogen events, but also:

1) A background of accidental coincidences.
2) Accidental coincidences from carbon.
3) Systematic coincidences from carbon.
4) Systematic inelastic coincidences from hydrogen.
5) Accidental "mixed" coincidences from (inelastic or elastic) hydrogen events arriving in one counter and carbon events in the other.

The coincidences from CH_2 were counted for unit integrated beam ("integrator volt"). The carbon target was then inserted, and coincidences from it were recorded for an integrator volt. The same was finally done with no target in the beam ("blank"). If we call H the number of coincidence counts due to hydrogen per integrator volt, we have:

$$H = CH_2 - zC - (1 - z)bl. \qquad (14)$$

It is clear that z is a function of the ratio of the surface density of the carbon target to that of the carbon in the CH_2 target, of the duty cycle of the deuteron beam, of the photomultiplier voltages and discriminator settings, and of the angles θ and Ⓗ involved.

Three methods were used to obtain z.

1) From Fig. 5 we see that the flat portion of the angle variation curve falls off quite sharply, so that there exists a region to either side of the flat portion where H should go to 0. By taking z somewhat greater than unity it was possible to make H go to zero there within statistical accuracy. The disadvantages of this method are that it is slow, lacks accuracy, and has to be applied in every region of angles covered during a particular day.

2) Counts were taken with both CH_2 and C targets as a function of beam current. Systematic coincidences are proportional to the current, accidental ones proportional to the current squared, or if counted for unit charge, independent of and linear in the current, respectively. In Fig. 9 is shown a sample plot of C and CH_2 coincidences as a function of beam intensity. The points were assumed to lie on two straight lines, and the factor z was defined as one that, when multiplying the carbon ordinates, would yield a straight line parallel to that passing through the CH_2 points. Thus, with proper z, H could be made independent of the beam current. Strictly speaking the blank count should have been included, but the change in z due to it was found negligible. This method, although potentially more accurate than the first, again suffered from the fact that it had to be applied in several regions of angle.

3) The single counting rates were used to find the carbon subtraction z. The problem could be treated algebraically to sufficient approximation if one assumed that the coincidence counting rates were small compared to the single

counting rates. It is shown in the appendix that:

$$z \approx R + \frac{2\tau}{p}\left[\frac{v_1 v_2}{X} - R u_1 u_2\right] \tag{15}$$

where $\underline{v}_1$, $\underline{v}_2$ are the single counting rates of channels 1 and 2 from CH_2, $\underline{u}_1$, $\underline{u}_2$ are the single counting rates of channels 1 and 2 from C, $\underline{R}$ is the ratio of the surface density of the carbon in the CH_2 target (close to 6/7 that of the CH_2) to that of the carbon target, $\underline{p}$ is the coincidence counting rate with carbon target, $\underline{X}$ is the ratio of the average beam current that obtained with the CH_2 target in the beam to that with the C target in the beam, and $\underline{\tau}$ is the "effective" resolving time of the coincidence circuit. $\underline{\tau}$ is defined by the equation:

$$s = 2\tau w_1 w_2 , \tag{16}$$

where $\underline{s}$ and $\underline{w}_1$, $\underline{w}_2$ are the coincidence, and single counting rates, respectively, with no target. It is a resolving time characteristic of the speed of the coincidence circuits and of the duty cycle of the beam. Since $\underline{\tau}$ was usually of the order of 5×10^{-5} sec. and the duty cycle of the beam of the order of 1/500, the resolving time of the coincidence was of the order of 10^{-7} sec.

Two methods for measuring $\underline{\tau}$ were used. One method was the direct evaluation of the quantities in Eq. (16). The other consisted of plotting carbon coincidences per integrator volt as a function of beam current. A sample plot is shown in Fig. 10. The resolving time was then given by dividing the slope of the curve by twice the product of the true single counts per integrator volt.

It should be pointed out that to obtain true single counts and true single counting rates slight corrections had often to be made due to counting losses attributable to the finite resolving time of the scalers. Usually the counting rate was kept below 120/sec., where the corrections amounted to less than 3 percent.

Method 3) was the most desirable one for determining z. Apart from $\mathcal{I}$, which was measured perhaps twice during a run to check that the cyclotron beam duty cycle had not changed, no special variation curves at various angles had to be taken. Besides being speedy, the method was also fairly accurate since it amounted, by Eq. (15), to finding a correction term to z = R. Usually it was found that $R \leq z \leq 1.2$, in agreement with the other methods.

B. SINGLE COUNT METHOD.

As $\Phi \to 0$, the proton acquires enough energy to have a greater range than the deuterons from the beam and from carbon. A single crystal and a variable amount of Al absorber much larger in area than the crystal were therefore used in this region. We give as an illustration the energies and ranges of some of the particles seen by the crystal at small angles.

TABLE I.

Angles and energies of deuterons and protons resulting from elastic scattering of 192 Mev deuterons on hydrogen, in which one of the particles scatters to near 0° in the laboratory; calculated with the relativistic relations of Sec. IV. Φ and Θ are angles of deflection of proton and deuteron, respectively, in the laboratory system; θ is the angle of deflection in the center of mass system. Energies are in Mev, ranges in g cm^{-2} of Al.

Φ	Θ	θ	PROTON Energy	PROTON Range	DEUTERON Energy	DEUTERON Range	$\left\lvert \frac{d \cos \Phi}{d \cos \theta} \right\rvert$	$\left\lvert \frac{d \cos \Theta}{d \cos \theta} \right\rvert$
0°	0°	180°	172	25.4	20	0.33	0.229	1.046
5°	10.3°	169.5°	170	25.0	22	0.39	0.230	0.913
10°	18.8°	159.2°	166	24.0	26	0.52	0.234	0.625
15°	24.7°	148.7°	159	22.4	33	0.81	0.240	0.356
65.5°	15°	47.1°	28	1.04	164	14.5	0.639	0.107
73.8°	10°	31.1°	13	0.26	179	16.8	0.966	0.107
82.0°	5°	15.4°	3	0.02	189	18.3	1.956	0.106
90°	0°	0°	0	0.0	192	18.9	∞	0.106

Here again proper precautions were taken.

1) Film was exposed to check on the alignment of our table.

2) A crystal plateau was taken by using the coincidence method for elastic scattering at angles appropriate for such scattering.

3) The validity of the beam integration with thick targets was checked by placing the ionization chamber at several distances from the target.

No problem arose from the carbon subtraction, since now $\underline{z} \equiv \underline{R}$. Account had to be taken of the fact that with a given amount of absorber in front of the single crystal the particles were stopped a different amount for the CH_2 and C targets and the blank. Thicker targets, of the order of a gram, were needed here to separate the hydrogen effect from a large background coming directly from the collimator. Since the inherent beam straggling (see Fig. 8) amounted to about 1 g of aluminum, the use of targets of this thickness was not expected to increase the straggling of the elastic protons and high energy deuterons by more than 15 percent. A plot of $\underline{H}$, true hydrogen counts per I.V., versus absorbing material at $\Phi = 10^{\circ}$, is shown in Fig. 11. The various particles could be identified by their ranges. A comparison of Fig. 11 with a similar plot of carbon vs. absorber and background vs. absorber showed that the elastic protons were clearly resolved from a long range background and lower energy particles. Furthermore the deuterons from carbon and from the beam caused sharp drops in the $\underline{C}$ and $\underline{bl}$ curves with the expected amount of absorber. Finally, as seen from Fig. 11, the elastic deuterons of 181 Mev were also clearly identified. It was therefore possible, by this method, to obtain the cross sections for small and large Θ for which the coincidence technique was unsuited. The relatively large background, which did not decrease appreciably with increasing absorber, was believed to be due to high energy

deuterons which strip in the aluminum before stopping. The proton is stopped, but the neutron may go on to make a knock-on proton in the region of absorber close to the crystal.

VI SAMPLE CALCULATION

A. Cross Section.

Once z has been found, $H = CH_2 - zC - (1 - z)bl$ is computed. The differential cross section is then given by:

$$\sigma(\Phi) = \frac{H}{n\ N\ \Delta\Omega}, \tag{17}$$

where $\Delta\Omega$ is the solid angle subtended by the proton crystal at angle Φ, N is the number of hydrogen atoms per cm^2 in the CH_2 target measured in the direction of the incident beam,

$$N = N_o \frac{2.016}{14.03} \frac{t}{\sin(\delta + \Theta)},$$

where N_o is Avogadro's number, 6.02×10^{23}, and t is the target thickness in g/cm^2; with H measured for one integrator volt, n is the number of incident deuterons required to charge a condenser of capacitance C connected to the collecting grid of the monitoring chamber to one volt. C was usually 0.99 or 0.0102 μf including capacitance of cables and chamber. Thus $n = \frac{C}{e\ \mu}$ where e is the electronic charge in Coulombs, μ is the multiplication of the argon filled ion chamber. μ was determined by calibrating the chamber against a Faraday cup for 345 Mev protons (cf. CSW) and using the range-energy relations of Aron, et al.[33] to convert to deuterons. The standard value obtained was $\mu = 1776$ at 20° C and a pressure of 76.5 cm Hg.

Finally, Eq. (17 was converted to the center of mass by using

$$\sigma(\theta) = \frac{d \cos \Phi}{d \cos \theta} \sigma(\Phi \tag{18}$$

where $$\frac{d \cos \Phi}{d \cos \theta} = \frac{A^2}{4 \cos \Phi} \left(1 + \left[\frac{1}{A^2} - 1\right] \cos^2 \Phi\right)^2 . \qquad (19)$$

B. Coincidence Method.

Here we shall pick out a set of data applying to $\Phi = 45^\circ$, taken on the same day as Fig. 10. We had, for one of several cycles of alternating $\underline{CH_2}$, $\underline{C}$ and $\underline{bl}$ sequences,

u_1 =	91.4 counts/sec.	$\underline{CH_2}$ =	61.0 ± 4.5
u_2 =	3.60 counts/sec.	$\underline{C}$ =	7.0 ± 1.5
v_1 =	103.0 counts/sec.	$\underline{bl}$ =	1 ± 1
v_2 =	4.91 counts/sec.	γ =	$(1.5 \pm 0.3) \times 10^{-5}$
X =	1.028		
p =	0.049 ± 0.010 counts/sec.		

Targets used were: CH_2 0.290 g cm^{-2}, C 0.338 g cm^{-2}, so $\underline{R}$ = 0.735.

From Eq. (15),

$$z = 0.89 \pm 0.04.$$

Therefore $\underline{H} = 61.0 \pm 4.5 - (0.89 \pm 0.04)(7.0 \pm 1.5) - (0.11 \pm 0.04)(1 \pm 1)$

$= 55 \pm 5.$

At $\Phi = 45^\circ$, $\Theta = 26.8^\circ$ and δ was 25°. Thus

$$N = 6.02 \cdot 10^{23} \frac{2.016}{14.03} \frac{0.290}{\sin 51.8^\circ} = 3.13 \cdot 10^{22} \text{ atoms cm}^{-2}.$$

Furthermore, $\underline{b}$ = 64.2 cm and the area of the crystal at angle Φ was $9.88(\pm 0.10)$cm^{-2}, so

$$\Delta\Omega = 2.40 \times 10^{-3} \text{ sterad.}$$

Ion chamber pressure was 78.4 cm at 23° C, so μ = 1801, $\underline{C} = 1.021 \times 10^{-7}$ f, hence $\underline{n} = 3.54 \times 10^8$ deuterons per integrator volt. From Eq. (17) we then obtain:

$$\sigma(\Phi = 45^\circ) = 2.07 \pm 0.19 \text{ mb sterad.}^{-1}$$

From Eq. (19), $\frac{d \cos \Phi}{d \cos \theta} = 0.354$ at $\Phi = 45^\circ$, $\theta = 87.5^\circ$.

Hence we finally have:

$$\sigma (\theta = 87.5^\circ) = (0.73 \pm 0.07) \cdot 10^{-27} \text{ cm}^2 \text{ sterad.}^{-1}$$

C. Single Count Method.

Here we shall choose $\Phi = 10^\circ$ (or $\Theta = 10^\circ$) for illustration.

1. General.

Targets used were CH_2 0.991 g, C 1.284 g. The latter was equivalent in stopping power to 1.67 g/cm^2 Al, the former to 1.53 g/cm^2 Al, so a slight extrapolation had to be made. The results are given in Fig. 11, where the relation (14) was used, with $z = 0.661$. Here the targets were oriented perpendicular to the beam. A thin Al wedge was centered over the crystal to make the energy of the particles entering the crystal equal over its surface.

2. $\Phi = 10^\circ$. From Fig. 12, the average background, for absorber > 24.0 g cm^{-2}, was 440 ± 50.

To find the proton effect we took the difference between the last point for which all the elastic protons seemed to come in, and the background. The error assigned was the statistical error of the point compounded with that of the background.

Again from Fig. 11, H at 22.9 g cm^{-2} Al equivalent of absorber was: 1830 ± 110 counts/I.V.

Net proton effect: $H = 1830 \pm 110 - 440 \pm 50 = 1390 \pm 120$.

Now $N = 8.58 \times 10^{22}$ atoms/cm^2 with $\sin(\delta + \Theta) = 1$;

$b = 100$ cm and the crystal area $= 9.55$ cm^2.

So $\Delta\Omega = 9.55 \times 10^{-3}$ sterad.

The ion chamber pressure was 77.4 cm Hg at 22° C, so $\mu = 1784$; $C = 0.99 \times 10^{-6}$ f, hence $n = 3.43 \times 10^9$ deuterons/volt, and

$$\sigma (\Phi = 10^\circ) = 4.95 \pm 0.43 \text{ mb sterad.}^{-1}$$

From Table I $\frac{d \cos \Phi}{d \cos \theta} = 0.234$ at $\Phi = 10^\circ$, $\theta = 159.2^\circ$.

Hence we finally have, in the center of mass, using Eq. (18),

$$\sigma(\theta = 159.2^\circ) = (1.16 \pm 0.10) \cdot 10^{-27} \text{ cm}^2 \text{ sterad.}^{-1}$$

3. $\Theta = 10^\circ$

We take the last point for which all the elastic deuterons seemed to come in, and subtract a background averaged over the first point with good statistics for which no such deuterons seemed to reach the crystal. This gives for the net deuteron effect:

$$H = (21200 \pm 700) - (2800 \pm 200) = 18400 \pm 750.$$

With the same values as above for n, N and $\Delta\Omega$,

$$\sigma(\Theta = 10^\circ) = 66.5 \pm 2.7 \text{ mb sterad.}^{-1}$$

From Table I

$$\frac{d \cos \Theta}{d \cos \theta} = 0.107 \text{ at } \Theta = 10^\circ, \theta = 31.1^\circ$$

so that, from Eq. (18), in the center of mass

$$\sigma(\theta = 31.1^\circ) = (7.0 \pm 0.3) \cdot 10^{-27} \text{ cm}^2 \text{ sterad.}^{-1}$$

It is clear that, apart from systematic errors discussed in the next section, the cross section at $\Phi = 10^\circ$ is an <u>upper limit</u>, inasmuch as some inelastic protons may be included. For if one assumed a just inelastic d-p collision with one proton going forward at high energy and the other proton and neutron remaining close neighbors, the energetic proton would have only of the order of 3 Mev less energy than an elastically scattered one in the forward direction. The cross section for elastic deuterons at $\Theta = 10^\circ$, on the other hand, is likely to be too low because of stripping losses. If we take[34] the stripping cross section as 150 mb for Al, we expect to lose 5 percent of the deuterons. Thus $\sigma(\theta = 31.1^\circ)$ should be raised 5 percent to give 7.4 ± 0.3 mb sterad.$^{-1}$

VII PRESENTATION OF DATA AND DISCUSSION OF ERRORS

The data are summarized in Table II. They have been averaged for a given angle over a given day's run, but results for the same angle obtained on a different day have been included separately. Cross sections for angles less than 1° different from those for a given listed angle have been included among the latter. Values marked with asterisks have been done with the single count method, all others with methods I-III.

TABLE II

Differential scattering cross section, $\sigma(\theta)$, in the center of mass system, in cm^2 sterad.$^{-1}$, as a function of θ, angle of deviation in the center of mass. Columns 2 and 3 give all experimental values together with their statistical errors; columns 4 and 5 list average values for given angles, together with their total (statistical + systematic) errors. Data marked * were taken by means of method IV.

θ, degrees	$\sigma(\theta)$	r.m.s. Stat. Error	$\overline{\sigma(\theta)}$	r.m.s. Total Error
15.4	25.4*	3.0	25.4	4.4
31.1	7.4*	0.3	7.4	1.0
38.4	6.6	0.4		
	4.9	0.6		
	4.8	0.3	5.3	0.5
48.1	4.4	0.3		
	4.6	0.3		
	3.13*	0.13	3.8	0.4
57.8	2.75	0.12		
	2.18	0.12		

TABLE II (continued)

θ, degrees	σ(θ)	r.m.s. Stat. Error	$\overline{\sigma(\theta)}$	r.m.s. Total Error
57.8	2.14	0.07		
	2.54	0.11	2.33	0.21
67.6	1.22	0.05	1.22	0.10
77.5	1.16	0.06	1.16	0.10
81.5	0.89	0.05	0.89	0.08
87.5	0.70	0.03		
	0.77	0.08	0.71	0.06
97.5	0.59	0.04		
	0.73	0.05	0.64	0.05
107.6	0.61	0.03	0.61	0.05
117.8	0.52	0.08	0.52	0.09
128.0	0.55	0.17		
	0.67	0.06		
	0.67	0.18		
	0.55	0.13		
	0.73	0.10		
	0.57	0.06		
	0.54	0.05		
	0.45	0.04	0.55	0.04
138.4	0.72	0.24		
	0.27	0.09		
	0.42	0.06		
	0.42	0.08	0.40	0.05

TABLE II (continued)

θ, degrees	σ(θ)	r.m.s. Stat. Error	$\overline{\sigma(\theta)}$	r.m.s. Total Error
148.7	0.27	0.23		
	0.51	0.25		
	0.67	0.07		
	0.62	0.12		
	0.24	0.14		
	0.52*	0.06		
	0.47*	0.07	0.54	0.07
159.2	1.45	0.50		
	1.16*	0.10	1.20	0.20
169.5	1.30*	0.23	1.30	0.29

Fig. 12 shows a plot of the results listed in Table II, center of mass cross sections along the ordinate, center of mass angle along the abscissa. Fig. 13 shows the weighted mean cross sections together with the curve used to find a total cross section from 10° to 180° in the center of mass of 29 ± 3 mb. The errors quoted in Fig. 12 and Table II are r.m.s. deviations due to statistics alone. Those of Fig. 13 include systematic uncertainites.

Among the most important systematic (r.m.s.) errors we should list:

1. Geometry.

a) The calibration of the scattering table was believed to be good to better than 1/2°.

b) The table alignment was accurate to about 1°; the alignment was checked by an angle variation curve of somewhat greater accuracy.

c) The distance b was measured from the center of the target, presumably coincident with the center of the beam, to the face of the crystal. Due to oblique orientation of the target, the error in b due to poor alignment could amount to 1/2 cm. Another uncertainty of the order of mm arose in the fact that the distance to which a particle had to enter a crystal before producing scintillation sufficient to give rise to a count was not known. b was usually between 50 and 100 cm.

d) The orientation of the targets with respect to the beam could be measured to better than 1° with a resulting r.m.s. error of 1.5 percent in the cross section.

e) The crystal area was known in all cases to be better than 2 percent.

f) The sensitivity of the crystals may not have been uniform over their surfaces. Although photomultiplier voltage plateaus and the use of different crystals at the same angles convinced us that within the counting statistics the crystals were uniformly sensitive, an uncertainty of 3 percent should be assigned to this factor.

g) Choice of solid angles: the non-defining crystal was always close enough to satisfy the geometric requirements and allow for a safety margin. The loss of coincidences due to this factor could not have amounted to more than 2 percent.

2. Beam Current Measurement.

a) Calibration. The calibration of the argon-filled ion chamber against a Faraday cup built by Dr. V. Z. Peterson has been described by CSW. This calibration was thought accurate to 1 percent.

b) Saturation. The chamber was run at 1000 V, high enough to measure better than 99 percent of the saturation current at any beam strength we used.

3. Multiple Scattering.

a) In methods I-III, multiple scattering in the targets could have resulted in a loss of 2 percent of the elastic events, except at $\Phi = 60^{\circ} - 70^{\circ}$, where the loss may have amounted to as much as 5 percent. In addition, in method III multiple scattering in the first of two crystals of a telescope could have caused some loss in the second, except that the latter was always chosen large enough to make such losses negligible.

b) In method IV the Al absorbers were large enough to result in "bad" geometry. Since, however, the cross section was not linear but had curvature in both regions investigated by this method, an uncertainty of 5 percent must be assigned to it due to multiple scattering in the absorbers.

4. Targets.

The polyethylene targets were analyzed (CSW) and shown to be of composition $(CH_2)_n$ to within 1 percent. The dimensions and weight, hence surface densities of the targets were known to 1 percent.

5. In methods I-III, losses due to finite resolving time of the coincidence circuit amounted to no more than 2 percent with the highest single counting rates used. In method IV similar losses due to finite scaler resolving times virtually cancelled since the counting rates were almost the same from CH_2, C, and bl, or else very low.

6. The method of finding z by measuring the single counting rates and the coincidence resolving time τ resulted in an uncertainty in the cross section of no more than 2 percent due to possible small variations in the cyclotron resolving time that might have passed unnoticed.

7. In all methods the possible inclusion of some inelastic d-p scattering caused some uncertainty. In methods I-III this may have amounted to 3 percent. In method IV, it may have been as high as 10 percent.

We summarize the systematic errors.

A. Methods I-III.

1.	c,d,e,f,g	: 5%
2.	a,b,c	: 2%
3.	a	: 2% (5%)
4.		: 1.5%
5.		: 2%
6.		: 2%
7.		: 3%

Total: 7% (9% at 60-70°)
Resolution: about 3° ave.
Angles certain to 2° in center of mass.

B. Method IV.

1.	c,e,f	: 3.5%
2.	a,b,c	: 5.5%
3.	b	: 5%
4.		: 1.5%
7.		: 10%

Total: 13%
Resolution: 2° or better
Angles certain to 2° in center of mass.

VIII CONCLUSIONS

Fig. 12 compares our results with those predicted by the theory of Chew.[1] Before discussing this comparison, we wish to say a few words about the theory. Chew assumed charge-independent, static central forces, with singlet and triplet "Serber potentials" representing the n-p interaction. The ranges and depths of the potential wells were those given in Sec. II. With such potentials the high energy n-p differential scattering cross section is quite well reproduced;[18] the high energy p-p differential scattering cross section predicted from the theory will have qualitatively the same shape[19] as the n-p cross section. This is, of course, not in agreement with experiment (CSW), but no experimental results were available in 1948. The first order Born approximation was thought to be sufficient; this was rendered quite convincing by the fact that the higher order impulse approximation[22] reduces to the Born approximation in the case of elastic d-p scattering. The identity of two of the nucleons involved, as well as the spin state restrictions due to the bound triplet state of the deuteron which must appear in both the initial and the final wave functions, were, or course, taken properly into account.

The final differential scattering cross section was then obtained in terms of the sum of the squares of the doublet and quartet interaction matrices with proper statistical weights. Each of the two matrices could be written as a linear combination of three terms I_1 I_2, I_3. Their coefficients in the matrices, as well as their numerical values, depended on the detailed description of the interaction, but their character was quite general. Thus I_1, the most important term, was the product of two probability amplitudes. One was the collision probability amplitude, its modulus square being the chance that either particle in the incident deuteron would strike the target

proton and thus impart to the struck particle a given momentum in a given direction. The second factor was the "sticking probability" amplitude, its modulus square being the chance that the two deuteron particles were still in their ground state after the collision. Both factors contributed a strong maximum in the forward direction near $\theta = 0^\circ$. I_2 had a very weak maximum at $\theta = 180^\circ$, and a moderately strong one at $\theta = 0^\circ$. It was the hardest to interpret; it reduced[36] to I_1 if one assumed that the range of the forces was negligible compared to the separation of the nucleons inside the deuteron. I_3 had a rather weak maximum at $\theta = 180^\circ$, and was the main contributor to the theoretical peak of Fig. 12 in that region. Its origin could be ascribed to a "pick-up" process in which the neutron of the incident deuteron collided with the target proton and formed a deuteron with it, while the proton initially in the deuteron proceeded forward with most of the kinetic energy. I_3 could be interpreted in terms of the product of three probability amplitudes;[37] one factor was the probability amplitude of the neutron of the incident deuteron having a certain internal momentum; the second factor was the probability amplitude of a collision between this neutron and the target proton, resulting in a certain final relative momentum and final momentum of the center of mass of the two particles involved in the collision; the third factor was the probability amplitude for this final relative momentum to be found in a bound deuteron. The last two factors were to be integrated over this final relative momentum, not an observable, and I_3 was the product of the resulting integral and the first factor.

We shall now compare our results with those predicted by Chew, and for this purpose (cf. Fig. 12) we shall subdivide the range of angles measured into three regions:

$$15^\circ \leqslant \theta \leqslant 50^\circ; \qquad 50^\circ \leqslant \theta \leqslant 130^\circ; \qquad 130^\circ \leqslant \theta \leqslant 170^\circ.$$

1. $15^\circ \leq \theta \leq 50^\circ$. Here the agreement is moderately good. Our points fall somewhat below the predicted ones. This may be due to the fact that Chew took a p-p interaction which gives a cross section higher than the observed one in this region.

2. $50^\circ \leq \theta \leq 130^\circ$. Here the agreement is excellent, in spite of the theoretically assumed p-p interaction, which would give too low a cross section in this region. The exact agreement is undoubtedly fortuitous, but both the theoretically assumed and the experimentally found cross sections vary slowly over these angles, so that the shape of the curve is dominated by the "sticking probability." The latter is critically dependent on the deuteron wave function chosen. In this region, where the internal momenta involved are moderate to fairly high, i.e., where the particles in the deuteron are fairly close together at the time of the collision, the wave function is probably not well enough known to give the sticking probability very accurately.

3. $130^\circ \leq \theta \leq 170^\circ$. Here the departure from Chew's predictions is quite marked. Our values near 170° are a factor of 4 to 5 lower than the theoretical ones. The disagreement may in part be due to our ignorance of the deuteron wave function in the region of zero separation of the two constituent nucleons. Indeed it can be shown[37] that the potential interaction between nucleons can be completely eliminated from I_3 in terms of the bound deuteron wave function by making use of Schroedinger's equation for the bound deuteron. Chew's choice for the wave function is

$$\psi_o = \frac{A}{r}\left(e^{-\alpha r} - e^{-\beta r}\right)$$

where $\underline{A}$ is a normalization factor, $\underline{r}$ the separation of the two nucleons, and $\underline{\alpha}$ and $\underline{\beta}$ are parameters adjusted by variation to give the binding energy when ψ_o is substituted in the Schroedinger equation for $\underline{l} = 0$ together with the triplet potential $V_t(r)$ of Sec. II. Since the maximum depth of the potential

is -67.8 Mev, an exact eigenfunction cannot yield Fourier components of internal momentum corresponding to a kinetic energy greater than 65.6 Mev, whereas our approximate eigenfunctions yield a spectrum without cut-off and varying as the inverse 8th power of the momentum. Thus a more correct eigenfunction may give a lower cross section for large θ. Conversely, experiments on p-d elastic scattering near $\theta = 180^\circ$ at various high energies (where the Born approximation is valid) may possibly tell us more about the deuteron wave function as $\underline{r} \to 0$, and hence about the potential $V_t(r)$.

It should also be mentioned that part of the discrepancy near $\theta = 180^\circ$ could be due to neglect of tensor forces,[38] which may, with suitable choice of potential, reduce the cross section in this region.

A comparison with Powell's[17] results reveals that our cross section is somewhat lower than his for both small and large θ. Part of the discrepancy may be due to systematic errors and normalization. It should, however, be pointed out that in the "pick-up" region even Powell's values are a factor of 3 lower than those predicted by Chew. In the region of intermediate θ, Powell's results and ours agree quite well, thus lending some support to the claim that nuclear forces are charge-independent, although considerably more work, both theoretical and experimental, is necessary before this hypothesis can become a fact. Our cross section between $\theta = 10^\circ$ and $\theta = 180^\circ$ is 29 ± 3 mb., as compared to Powell's total cross section of 46 mb. The discrepancy must not be taken too seriously, inasmuch as we have neglected contributions from $\theta < 10^\circ$, and Powell's normalization of all his elastic plus inelastic events to the n-d attenuation cross section of Cook et al.[39] may be subject to revision (cf. ref. 40).

The possibility of a repulsive core[20] in the singlet states should finally be mentioned. At high enough energies, the result of such a core would be

to reverse the sign of the singlet S-wave phase shift, at still higher energies that of the D-wave phase shift, etc. Thus the cross section in the central region of angles would be considerably lower than that calculated with a purely attractive potential, due to destructive interference between singlet and triplet scattering. Experiments on p-d scattering using 340 Mev protons are in preparation to explore these possibilities.

IX ACKNOWLEDGMENTS

The author wishes to thank Professor E. Segrè for continued interest and encouragement, and Professor Owen Chamberlain for many valuable suggestions and stimulating discussions on all phases of the work. He is indebted to Dr. Clyde Wiegand and Mr. A. L. Bloom for the design of some of the equipment, to Dr. R. F. Leininger for growing the stilbene crystals, and to Mr. A. L. Bloom and Professor Chamberlain for assistance in carrying out the experiments. The patience and ingenuity of the 184-inch cyclotron crew under Mr. James Vale were of inestimable value.

This work was performed under the auspices of the Atomic Energy Commission and was carried out in part while the author was Amy Bowles Johnson Memorial Fellow at the University of California.

X APPENDIX

Derivation of formula (15) of text.

We define the following symbols:

u_1, u_2 single counting rates from carbon target.

v_1, v_2 single counting rates from polyethylene target.

w_1, w_2 single counting rates from blank.

p coincidence counting rate from carbon target

q coincidence counting rate from CH_2 target.

s coincidence counting rate from blank.

R ratio of carbon surface density of CH_2 target to surface density of carbon target.

I_C integrator volts per second (beam current) during carbon measurement.

I_H integrator volts per second (beam current) during CH_2 measurement.

I_{bl} integrator volts per second (beam current) during bl measurement.

$$X = \frac{I_H}{I_C}$$

$$Y = \frac{I_H}{I_{bl}}$$

τ measured coincidence resolving time.

a_1, a_2 accidental single counting rates due to carbon.

b_1, b_2 accidental single counting rates due to hydrogen.

x systematic coincidence counting rate due to carbon.

y systematic coincidence counting rate due to hydrogen.

The last six quantities are not directly measurable and must not appear in the final expression for z.

If the beam currents for the CH_2, C and bl measurements are the same, we can write the relations,

(a) $u_1 = a_1 + w_1 + x,$

(b) $u_2 = a_2 + w_2 + x,$

(c) $v_1 = R(a_1 + x) + b_1 + y + w_1,$

(d) $v_2 = R(a_2 + x) + b_2 + y + w_2,$

(e) $p = x + 2\sigma(a_1 + w_1)(a_2 + w_2),$

(f) $q = Rx + y + 2\sigma(Ra_1 + b_1 + w_1)(Ra_2 + b_2 + w_2),$

(g) $s = 2\sigma w_1 w_2.$

If the beam currents are not the same, the counting rates have to be normalized to the same value, and we have,

$$\frac{u_1}{I_C} = \frac{a_1 + x}{I_C} + \frac{w_1}{I_{bl}}, \qquad \frac{u_2}{I_C} = \frac{a_2 + x}{I_C} + \frac{w_2}{I_{bl}};$$

$$\frac{v_1}{I_H} = \frac{R(a_1 + x)}{I_C} + \frac{b_1 + y}{I_H} + \frac{w_1}{I_{bl}}, \quad \frac{v_2}{I_H} = \frac{R(a_2 + x)}{I_C} + \frac{b_2 + y}{I_H} + \frac{w_2}{I_{bl}};$$

$$\frac{p}{I_C} = \frac{x}{I_C} + 2\sigma I_C\left(\frac{a_1}{I_C} + \frac{w_1}{I_{bl}}\right)\left(\frac{a_2}{I_C} + \frac{w_2}{I_{bl}}\right);$$

$$\frac{q}{I_H} = \frac{y}{I_H} + R\frac{x}{I_C} + 2\sigma I_H\left(\frac{R\,a_1}{I_C} + \frac{w_1}{I_{bl}} + \frac{b_1}{I_H}\right)\left(\frac{R\,a_2}{I_C} + \frac{w_2}{I_{bl}} + \frac{b_2}{I_H}\right).$$

Multiplying out, we finally obtain:

(h) $u_1 = a_1 + x + \frac{Y}{X} w_1, \qquad u_2 = a_2 + x + \frac{Y}{X} w_2;$

(i) $v_1 = XR(a_1 + x) + b_1 + y + Y w_1,$

$v_2 = XR(a_2 + x) + b_2 + y + Y w_2;$

(j) $$p = x + 2\gamma\left(a_1 + \frac{Y}{X} w_1\right)\left(a_2 + \frac{Y}{X} w_2\right);$$

(k) $$q = y + RXx + 2\gamma(RXa_1 + Yw_1 + b_1)(RXa_2 + Yw_2 + b_2).$$

Now, from Eq. (14), we define $\underline{y} = \underline{q} - \underline{zp} - (1 - \underline{z})\underline{s}$

or, in case the beam current varied,

$$\frac{\underline{y}}{I_H} = \frac{\underline{q}}{I_H} - \underline{z}\frac{p}{I_C} - (1 - \underline{z})\frac{s}{I_{b1}}$$

so that
$$z = \frac{q - y - Ys}{Xp - Ys}$$
$$= \frac{1}{Xp - Ys}\left[RXx + 2\gamma(RXa_1 + Yw_1 + b_1)(RXa_2 + Yw_2 + b_2) - Ys\right].$$

Eliminate $\underline{x}$ by using (j),

$$z = \frac{1}{Xp - Ys}\left[2\gamma(RXa_1 + Yw_1 + b_1)(RXa_2 + Yw_2 + b_2) + RXp - Ys - 2\gamma RX\left(a_1 + \frac{Y}{X} w_1\right)\left(a_2 + \frac{Y}{X} w_2\right)\right].$$

We now make the (for us always valid) assumption that $\underline{y}, \underline{x} \ll \underline{a}, \underline{b}, \underline{w}$, so that:

$$u_1 \approx a_1 + \frac{Y}{X} w_1, \text{ etc.};$$

$$v_1 \approx RXa_1 + Yw_1 + b_1, \text{ etc.}$$

Hence

(l) $$z \cong R + \frac{2\gamma}{Xp - Ys}\left[v_1 v_2 - RXu_1 u_2 - (1 - R)\, Yw_1 w_2\right].$$

Usually we had $Xp \gg Ys$, and $(1 - \underline{R})\, Yw_1 w_2$ negligible compared to the difference of the other two terms in [ ]. In that approximation Eq. (15) results.

XI REFERENCES

1. Geoffrey F. Chew, Phys. Rev. 74, 809 (1948)
2. H. A. Bethe and R. F. Bacher, Rev. Mod. Phys. 8, 82 (1936)
3. Breit, Condon, and Present, Phys. Rev. 50, 825 (1936)
4. John M. Blatt, Phys. Rev. 74, 92 (1948)
5. E. Fermi and L. Marshall, Phys. Rev. 71, 66 (1947)
6. J. M. Blatt and J. D. Jackson, Phys. Rev. 76, 18 (1949)
7. J. D. Jackson and J. M. Blatt, Rev. Mod. Phys. 22, 77 (1950)
8. L. W. Alvarez and K. S. Pitzer, Phys. Rev. 58, 1003 (1940)
9. Sutton, Hall, Anderson, Bridge, DeWire, Lavatelli, Long, Snyder and Williams, Phys. Rev. 72, 1147 (1947)
10. Hans A. Bethe, Elementary Nuclear Theory (Wiley, New York, 1947) p. 49
11. Hoisington, Share, and Breit, Phys. Rev. 56, 884 (1939)
12. G. Sachs and M. Goeppert-Mayer, Phys. Rev. 53, 991 (1938)
13. Birge, Kruse, and Ramsey, Phys. Rev. 83, 274 (1951)
14. Chamberlain, Segrè, and Wiegand (in press, Phys. Rev., hereafter referred to as CSW); see also Phys. Rev. 81, 919 (1951)
15. Oxley, Schamberger, and Towler, Phys. Rev. 82, 295 (1951)
16. Hadley, Kelly, Leith, Segrè, Wiegand, and York, Phys. Rev. 75, 351 (1949)
17. Wilson M. Powell (in press, Phys. Rev.)
18. R. S. Christian and E. W. Hart, Phys. Rev. 77 441 (1950)
19. R. S. Christian and H. P. Noyes, Phys. Rev. 79, 85 (1950)
20. Robert Jastrow, Phys. Rev. 81, 165 (1951)
    see also Phys. Rev. 81, 636 (1951), Phys. Rev. 79, 81 (1950)
    Phys. Rev. 79, 389 (1950), Phys. Rev. 82, 261 (1951)
21. K. M. Case and A. Pais, Phys. Rev. 80, 203 (1950)
22. Geoffrey F. Chew, Phys. Rev. 80, 196 (1950)
23. R. L. Gluckstern and H. A. Bethe, Phys. Rev. 81, 761 (1951)

p-d 3.5 MeV

24. Sherr, Blair, Kratz, Bailey, and Taschek, Phys. Rev. 72, 662 (1947)

25. L. Rosen and J. C. Allred, Phys. Rev. 82, 777 (1951)

26. H. S. W. Massey and R. A. Buckingham, Phys. Rev. 73, 260 (1948) p-d low en

27. J. H. Coon and R. F. Taschek, Phys. Rev. 76, 710 (1949) n-d 14 MeV

28. R. A. Buckingham and H. S. W. Massey, Phys. Rev. 71, 558 (1947) n-d

29. Charles E. Leith, Phys. Rev. 78, 89 (1950)

30. A. W. Vance, Rev. Sci. Inst. 7, 489 (1936)

31. Ginston, Hewlett, Jasberg, and Noe, Proc. IRE 36, 956 (1948)

32. Clyde Wiegand, Rev. Sci. Inst. 21, 975 (1950)

33. Aron, Hoffman, and Williams, AECU - 663

34. Robert Serber, Phys. Rev. 72, 1007 (1947)

35. R. W. Mather and E. Segrè (in press, Phys. Rev.)

36. O. Chamberlain, private comm.

37. G. F. Chew and M. L. Goldberger, Phys. Rev. 77, 470 (1950)

38. Horie, Tamura and Yoshida, private comm. (to be published in Progr. Theor. Phys.)

39. Cook, McMillan, Peterson, and Sewell, Phys. Rev. 75, 7 (1949)

40. J. DeJuren and N. Knable, Phys. Rev. 77, 606 (1950)

XII FIGURE CAPTIONS

Fig. 1 Schematic diagram of the cyclotron, deflecting magnet, and collimator.

Fig. 2 Block diagram of the electronic circuits of the experiment (method III of text) together with a top view of the coincidence apparatus.

Fig. 3 a) velocity diagram of a deuteron and a proton colliding in their center of mass, showing the definition of angle θ of the text.

b) The same collision, as viewed from the laboratory system; the distances b and c of the proton crystal and deuteron crystal from the target are shown, and the angles Φ, Θ and δ of the text are defined.

c) Criterion for the height of the larger, non-defining crystal, shown by projection of the arrangement of Fig. 3b onto a plane perpendicular to the beam. Orders of magnitude are typical of the operation at $\Phi = 40^\circ$.

Fig. 4 Coincidence counts per unit beam charge incident on the target ("integrator volt") at $\Phi = 25^\circ$ as a function of the height of the scattering table. CH_2 coincidences are circles, C coincidences are crosses. Operating height was taken as 0.1 cm, 0 cm being the height determined from use of the quadrant ion chambers.

Fig. 5 Coincidence counts per unit beam charge as a function of angle Θ, Φ being held constant to 45°. CH_2, ●; C, x. Operating angle chosen was 26°. Relativistic kinematics gives 25.8°, non-relativistic kinematics, 26.5°.

Fig. 6 Plateau of coincidence counts per unit beam charge versus photomultiplier voltage. CH_2 ●, C x, blank ■. Operating potential chosen: 750 V.

Fig. 7 Coincidences per unit beam as a function of Al absorber in front of the proton crystal at $\Phi = 40^\circ$. Expected range: 9.4 g cm^{-2}. CH_2 ●, C x.

Fig. 8 "Bragg curve" of the deuteron beam measured by taking the ratio of the integrated current of two argon-filled ion chambers as a function of aluminum absorber placed between them. Range at 0.8 of maximum height[35] is 18.8 g cm^{-2}, corresponding to an energy of 192 Mev. Straggling amounts to approximately 0.7 g cm^{-2}.

Fig. 9 Coincidence counts per unit beam charge of CH_2, ●, and C, x, as a function of beam current. The ratio of CH_2 slope to C slope determines the carbon subtraction ratio z, here about 1.1.

Fig. 10 Carbon coincidences per unit beam charge at $\Phi = 45^\circ$ as a function of beam current I. The finite intercept at I = 0 is due to systematic coincidences from carbon.

Fig. 11 Hydrogen counts per unit beam charge, obtained by subtraction, as a function of Al absorber in front of the crystal. (Method IV). Arrows a and b give the absorber, 16.7 g cm^{-2} and 24.2 g cm^{-2}, at which half the elastic deuterons (corresponding to $\Phi = 73.8^{\circ}$) and protons are counted. Calculated ranges are 16.8 g cm^{-2} and 24.0 g cm^{-2}, respectively.

Fig. 12 Differential elastic scattering cross section, in the center of mass, as a function of center of mass angle θ, showing almost all experimental points. Note folded scale to the left. For comparison the cross section calculated by Chew[1] is included.

Fig. 13 Averaged differential elastic cross sections in the center of mass, with their total (statistical and systematic) errors. The curve was used to find the total cross section between 10° and 180°, 29 ± 3 mb.

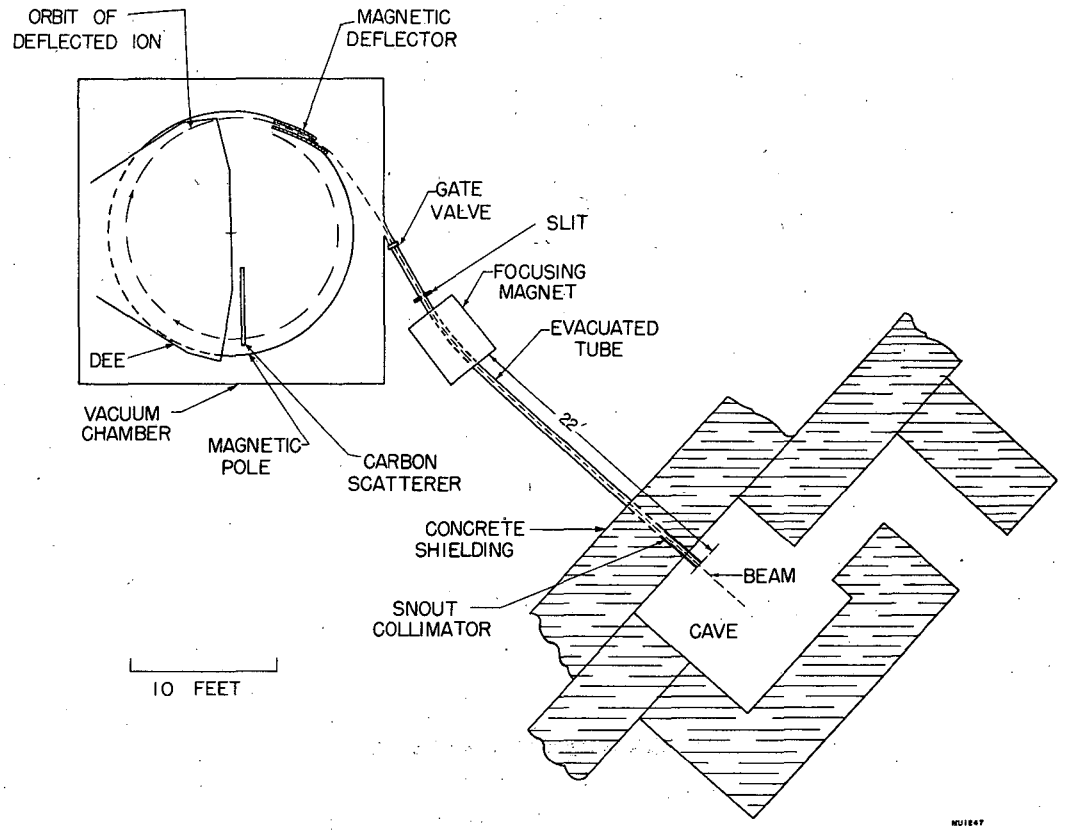
ORBIT OF
DEFLECTED ION
MAGNETIC
DEFLECTOR
GATE
VALVE
SLIT
FOCUSING
MAGNET
EVACUATED
TUBE
DEE
VACUUM
CHAMBER
MAGNETIC
POLE
CARBON
SCATTERER
22'
CONCRETE
SHIELDING
BEAM
SNOUT
COLLIMATOR
CAVE
10 FEET

Fig. 1

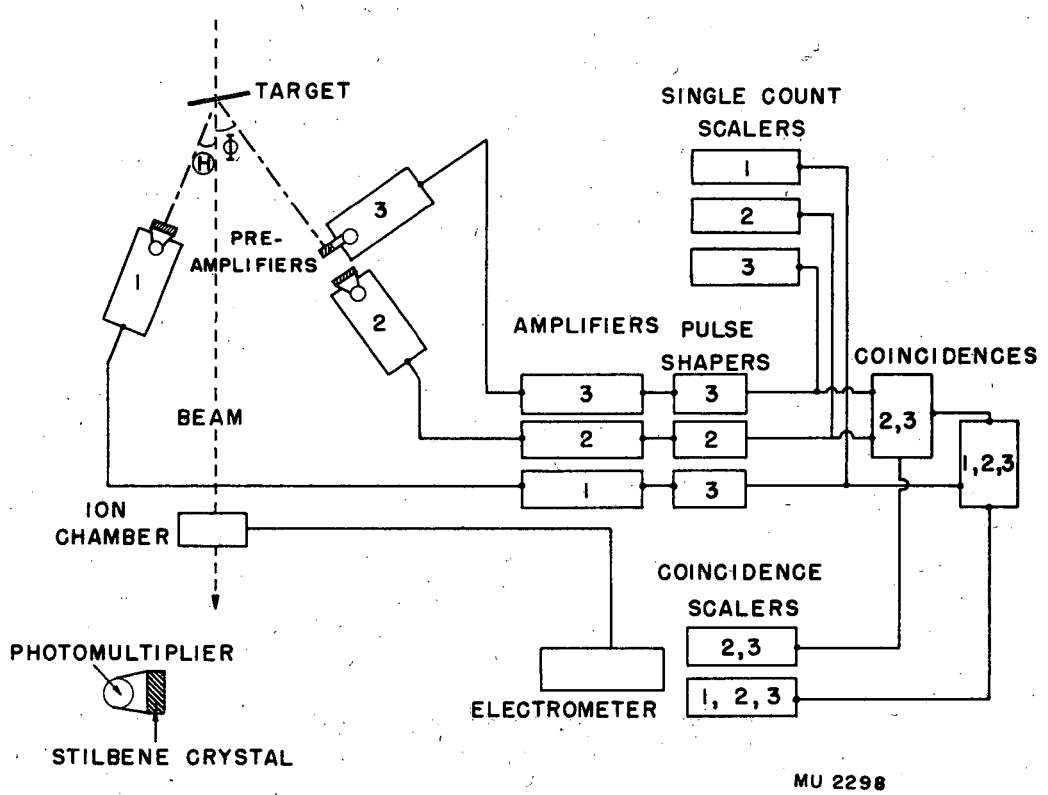
TARGET
SINGLE COUNT SCALERS
1
2
3
PRE-AMPLIFIERS
AMPLIFIERS
PULSE SHAPERS
COINCIDENCES
2,3
1,2,3
BEAM
ION CHAMBER
COINCIDENCE SCALERS
PHOTOMULTIPLIER
STILBENE CRYSTAL
ELECTROMETER
MU 2298

Fig. 2

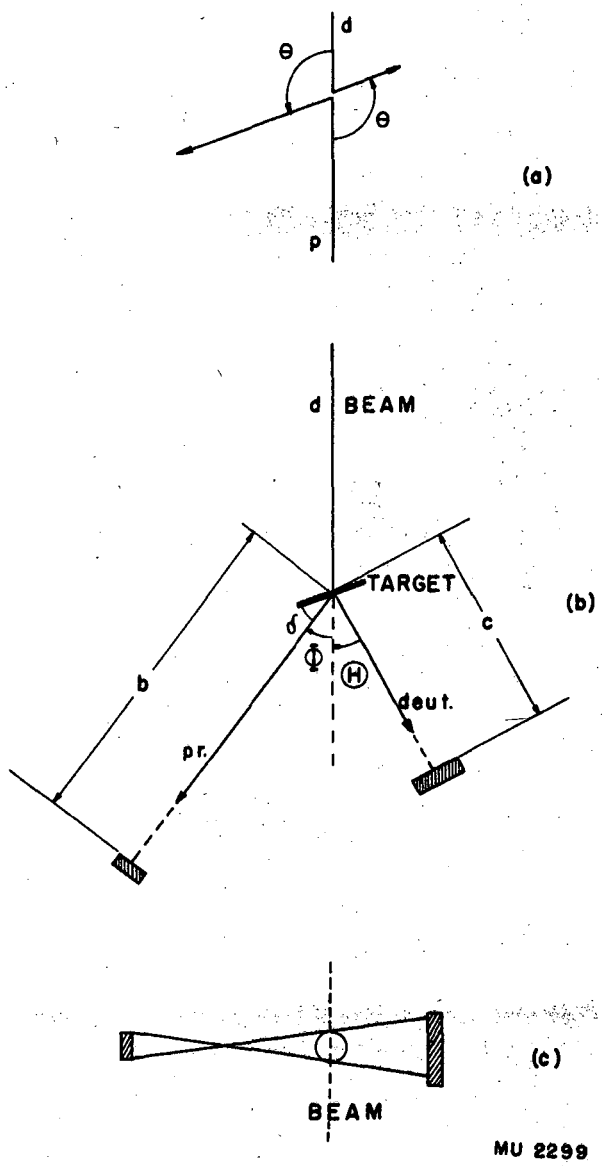

Fig. 3

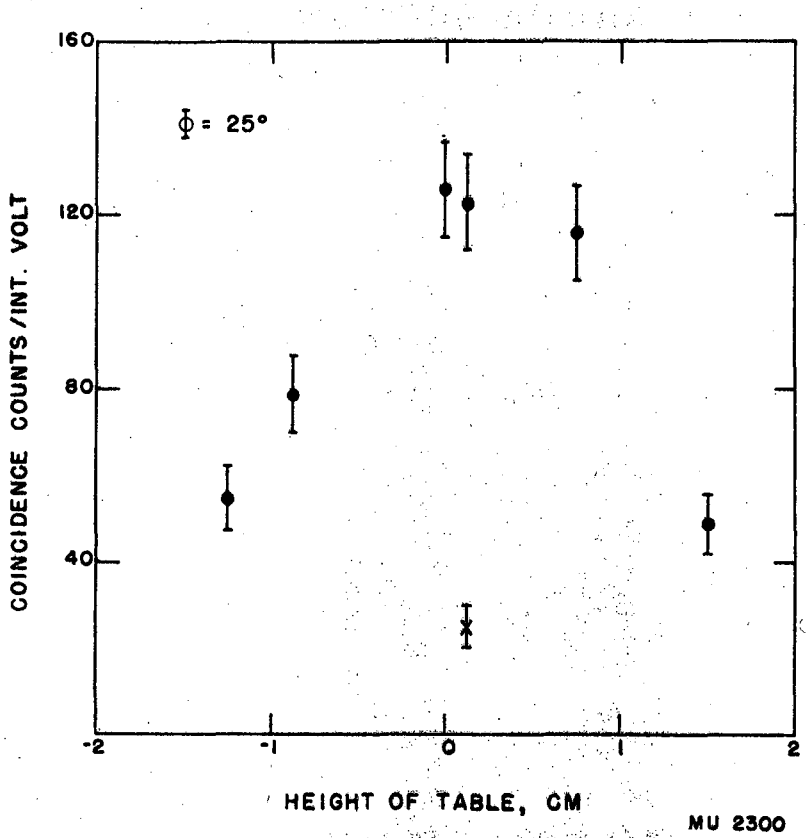
160
120
80
40
Φ = 25°
COINCIDENCE COUNTS/INT. VOLT
-2
-1
0
1
2
HEIGHT OF TABLE, CM
MU 2300

Fig. 4

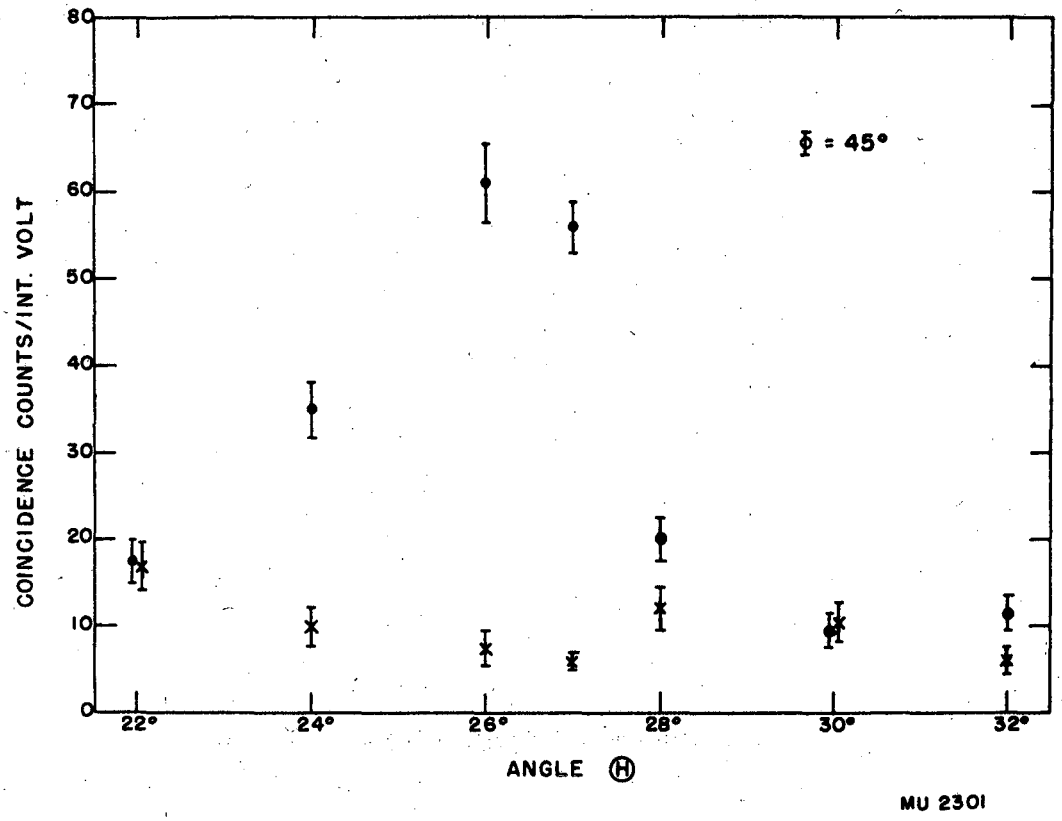
80
70
60
50
40
30
20
10
0
COINCIDENCE COUNTS/INT. VOLT
Φ = 45°
22°
24°
26°
28°
30°
32°
ANGLE Θ
MU 2301

Fig. 5

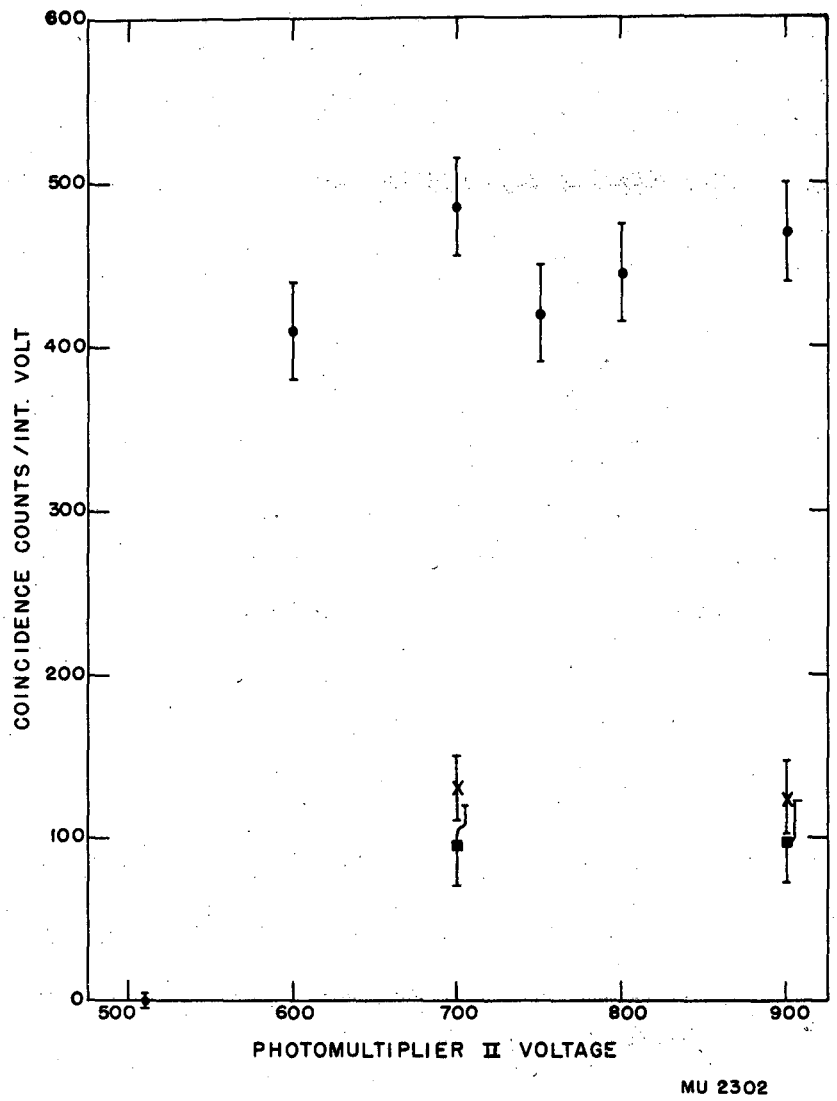
600
500
400
300
200
100
0
COINCIDENCE COUNTS/INT. VOLT
500
600
700
800
900
PHOTOMULTIPLIER II VOLTAGE
MU 2302

Fig. 6

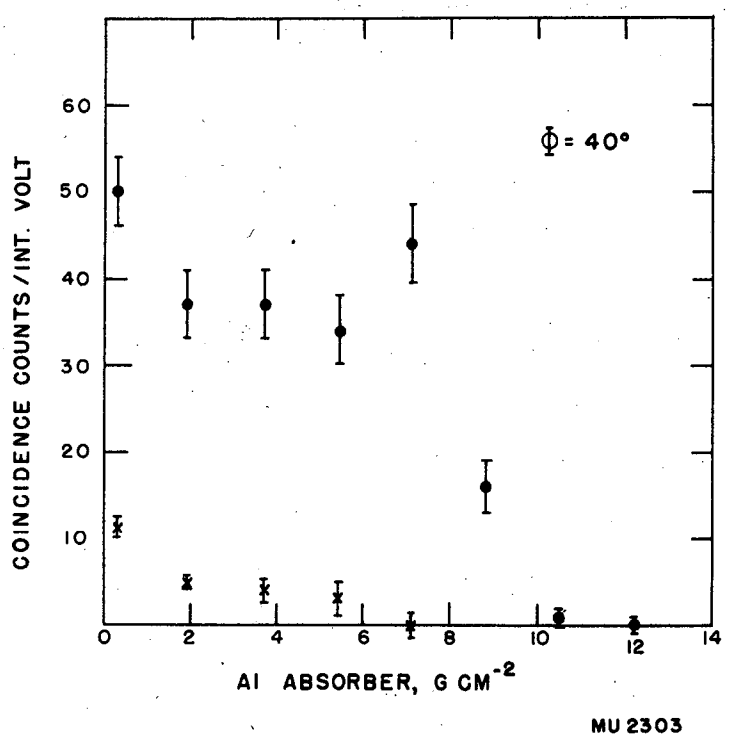
COINCIDENCE COUNTS/INT. VOLT
60
50
40
30
20
10
Φ = 40°
0
2
4
6
8
10
12
14
Al ABSORBER, G CM^{-2}
MU 2303

Fig. 7

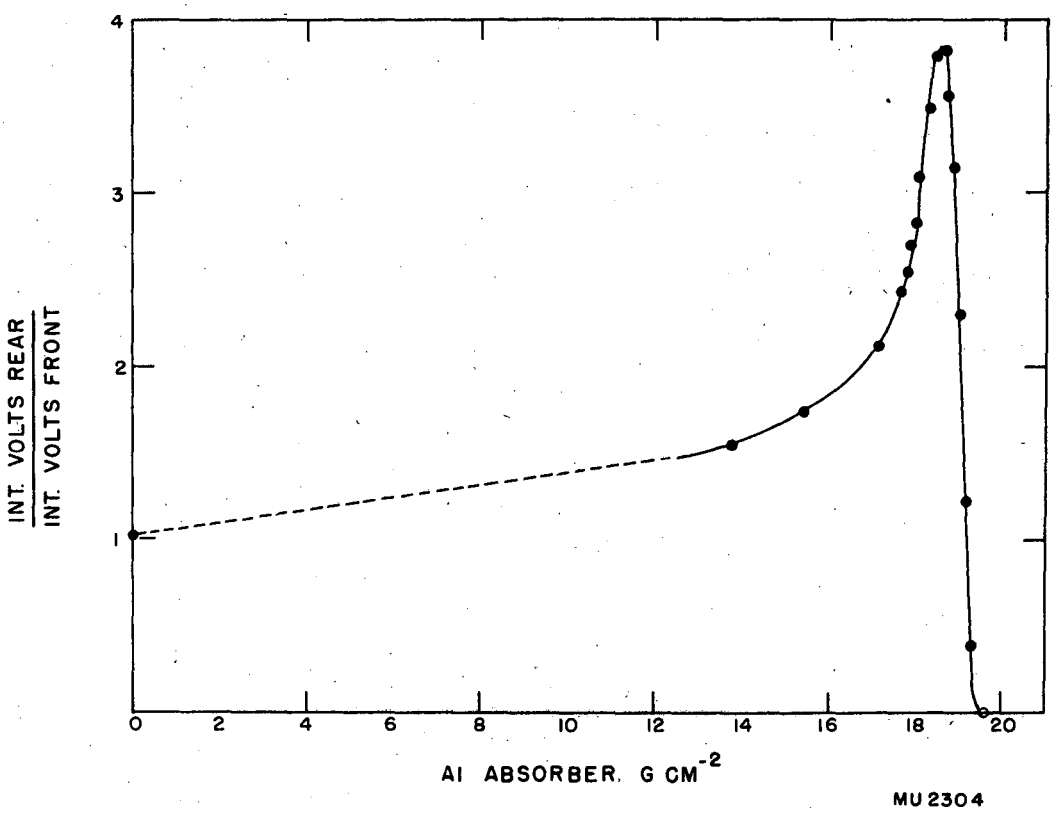
INT. VOLTS REAR / INT. VOLTS FRONT
4
3
2
1
0
2
4
6
8
10
12
14
16
18
20
Al ABSORBER. G CM^{-2}
MU 2304

Fig. 8

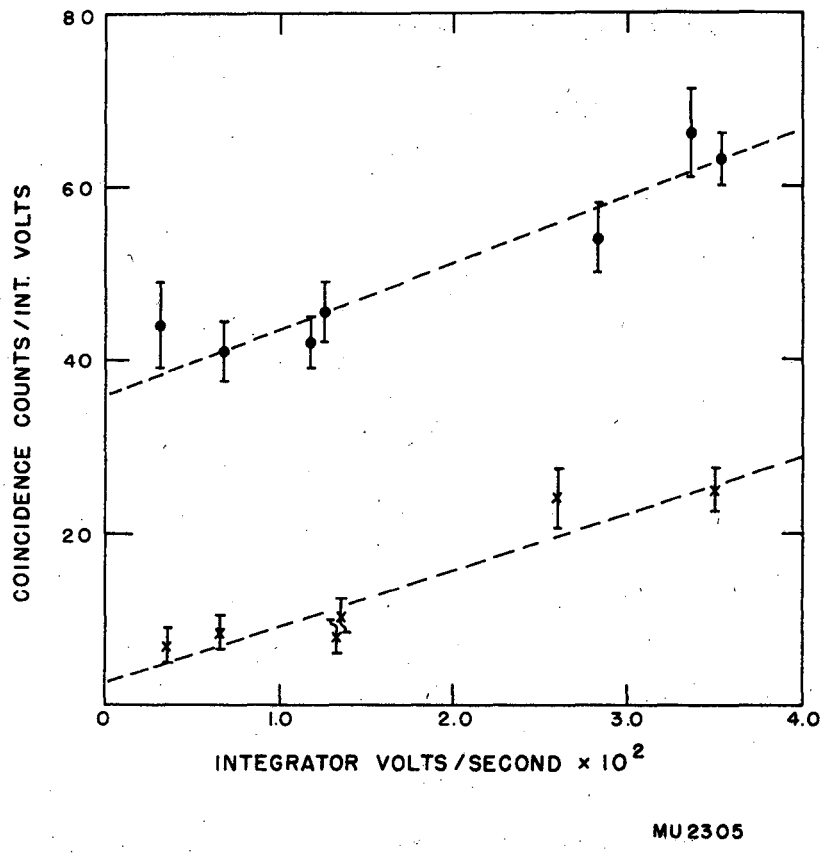
80
60
40
20
0
1.0
2.0
3.0
4.0
COINCIDENCE COUNTS/INT. VOLTS
INTEGRATOR VOLTS/SECOND × 10²
MU2305

Fig. 9

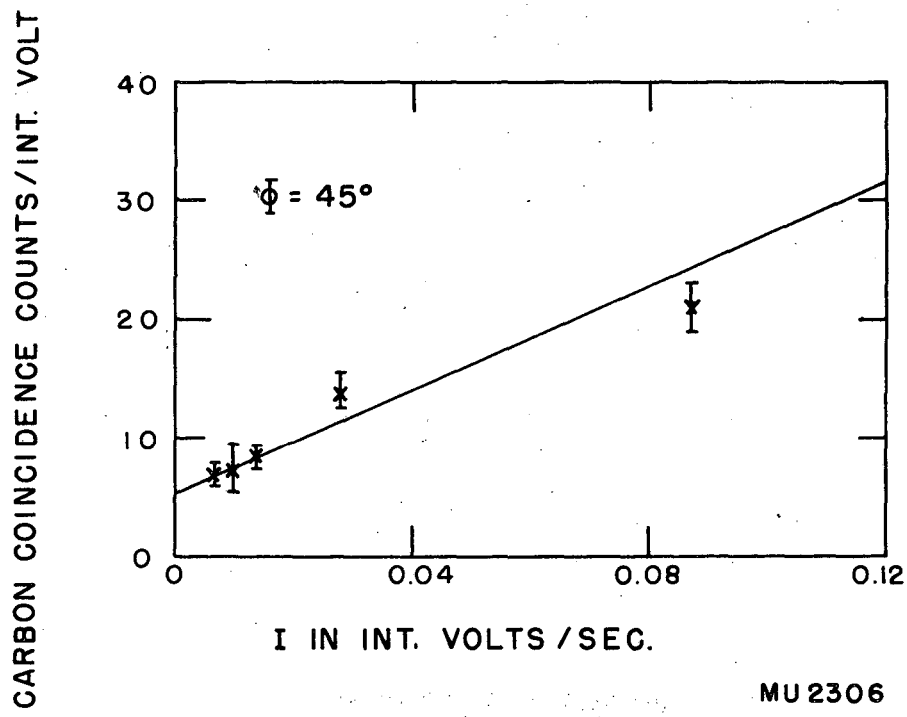
CARBON COINCIDENCE COUNTS/INT. VOLT
40
30
20
10
0
Φ = 45°
0
0.04
0.08
0.12
I IN INT. VOLTS/SEC.
MU 2306

Fig. 10

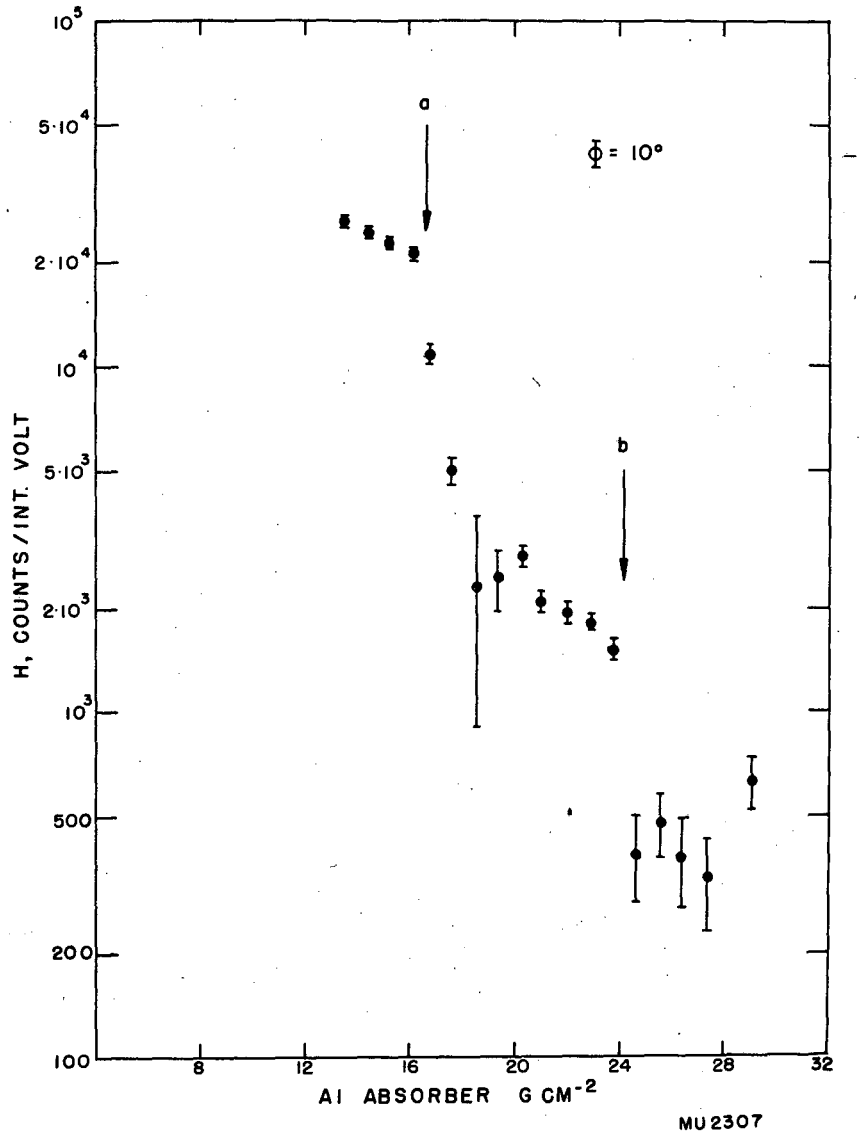
10^5
5·10^4
2·10^4
10^4
5·10^3
2·10^3
10^3
500
200
100
H, COUNTS / INT. VOLT
a
b
Φ = 10°
8
12
16
20
24
28
32
Al ABSORBER G CM^-2
MU 2307

Fig. 11

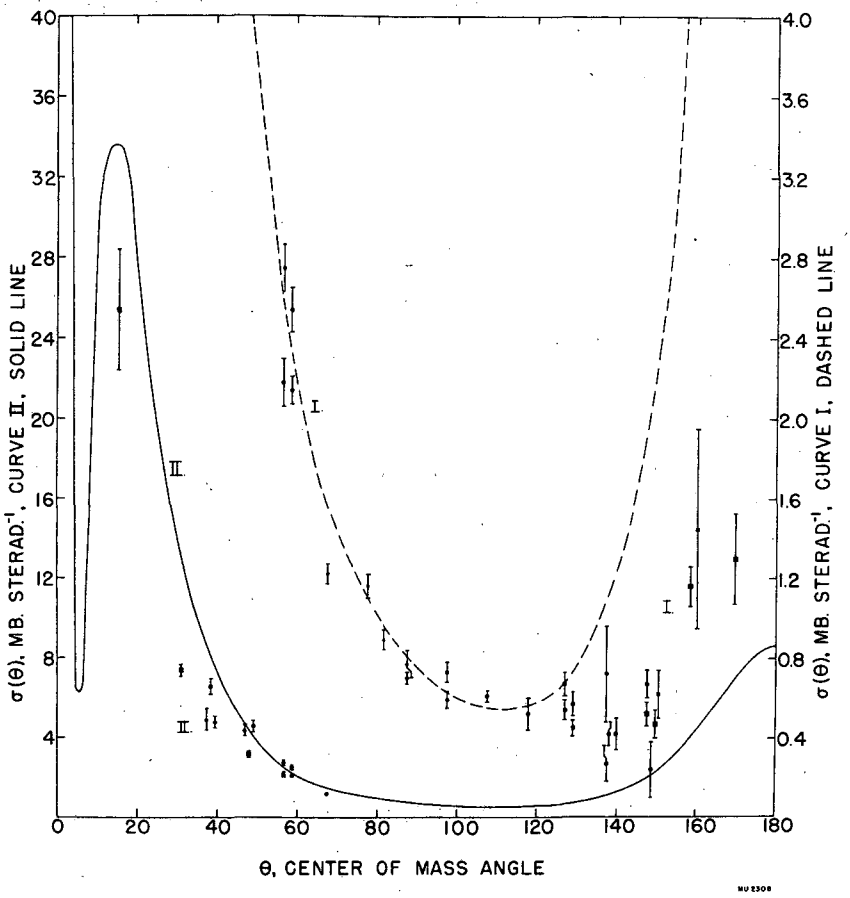
σ(θ), MB. STERAD.⁻¹, CURVE II, SOLID LINE
σ(θ), MB. STERAD.⁻¹, CURVE I, DASHED LINE
θ, CENTER OF MASS ANGLE
40
36
32
28
24
20
16
12
8
4
4.0
3.6
3.2
2.8
2.4
2.0
1.6
1.2
0.8
0.4
0
20
40
60
80
100
120
140
160
180
I
II

Fig. 12

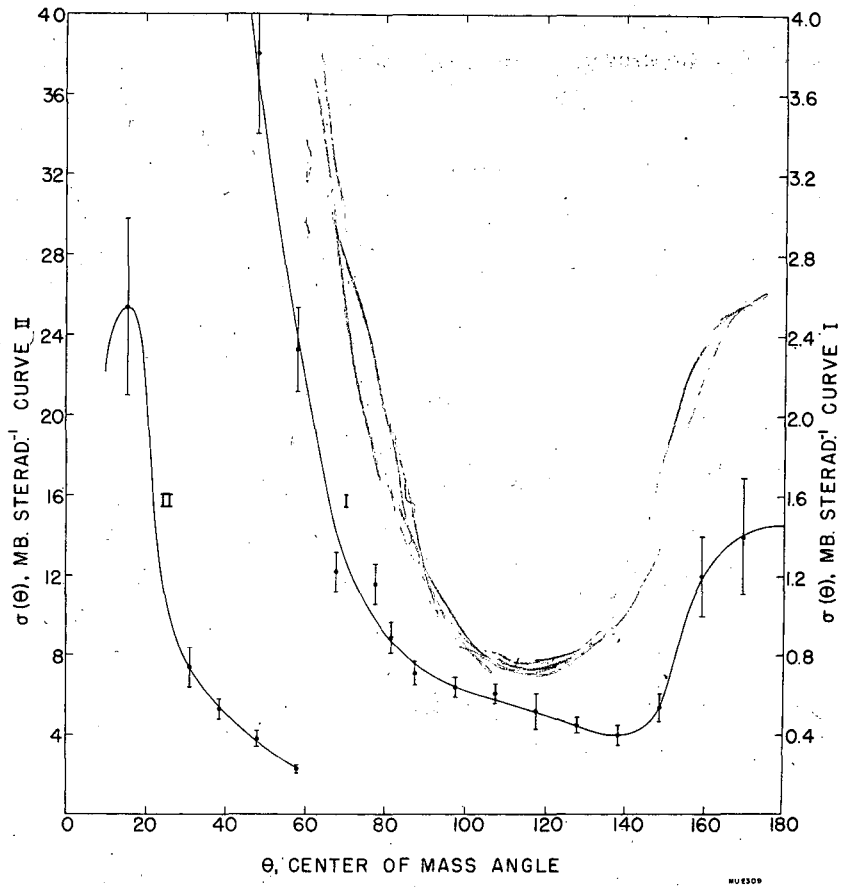
σ (Θ), MB. STERAD.⁻¹ CURVE II
σ (Θ), MB. STERAD.⁻¹ CURVE I
Θ, CENTER OF MASS ANGLE
II
I
0
20
40
60
80
100
120
140
160
180
4
8
12
16
20
24
28
32
36
40
0.4
0.8
1.2
1.6
2.0
2.4
2.8
3.2
3.6
4.0

Fig. 19